CHAPTER III

MITIGATING THE DETUNING EFFECTS OF BENDING

3.1 INTRODUCTION

A flexible antenna based on silicone-foam developed in Chapter II was evaluated for its bending performance (Section 2.6.3). The antenna was tested for bending along two directions, (I) bending axis perpendicular to the radiating edge of the patch and (II) bending axis parallel to the radiating edge. For Case I bending there was a shift of ~ 60 MHz towards the lower frequency side (simulation ~ 220 MHz) for bending radii 20mm was observed, while in Case II bending a shift of ~ 220 MHz (simulation ~ 90 MHz) towards higher frequencies was observed.

Efforts are made in the current chapter to mitigate the shift in frequency of the said antenna. Reports have employed auxiliary components to achieve frequency reconfiguration [1, 2, 3]. However, in the current work a self-compensating technique [4] i.e., without any externally aided systems, is employed. The mechanism for frequency compensation is based on variation of the effective dielectric constant (ε_{eff}) of the substrate. The idea is to engrave grooves into the flexible substrate in a way that the dielectric constant of the substrate gets modified. An optimization study in CST Microwave Studio is carried out by varying the groove count and the inter-groove distance to obtain the desired antenna performance. The optimized structure is then fabricated and experimentally verified. The design frequency for all the patch antennas in the current work is at 10 GHz which is the centre frequency of X-band so that any shift in the resonant frequency of the patch antennas does not intrude into the nearby bands.

3.2 SELF-COMPENSATION TECHNIQUE

The flexible silicone-foam multi-layered substrate with ε_{rs} = 2.19 and tanδ = 0.01 at 10 GHz is used in the current study. A modification is carried out by incorporating grooves in the substrate and injecting materials (ε_r) inside the groove to change the effective dielectric constant, ε_{eff}, of the substrate. A schematic of the substrate along with the incorporated groove is shown in Figure 3.1.

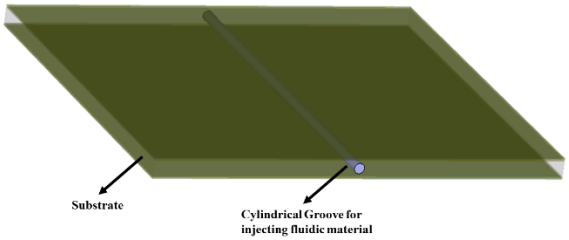

Figure 3.1 Schematic of the groove integrated substrate for patch antenna application

In Case I (as mentioned in the previous section), where the bending axis is perpendicular to the radiating edge, the frequency detunes towards the lower side, hence the material after insertion in the grooves must decrease the ε_{eff}, while for bending axis parallel to the radiating edge i.e., in Case II, inserted material should have $\varepsilon_r > \varepsilon_{rs}$, which will increase the ε_{eff}. Additionally, with bending there is a possibility of the change in shape of the groove. A detail study of both the aspects, material injection and shape variation on self-compensation is carried out.

3.2.1 Characterization of the injected material

The materials injected must be fluidic and self-healing in nature to comply with the bending curvatures. In Case I, air with $\varepsilon_r = 1$ ($< \varepsilon_{rs} = 2.19$) is taken. In Case II Ethylene Glycol (EGl) is considered. EGl (Make-Merck) is a non-toxic organic liquid which has good cohesion properties that makes it favourable for injecting it into the grooves without much surface resistance [16]. Permittivity studies in X-band is carried out on EGl at room temperature (25°C) using a dielectric probe kit (Keysight N1501A) compatible with a PNA series Agilent Vector Network Analyzer E8362C (VNA). The permittivity and loss tangent plots are shown in Figure 3.2. The dielectric permittivity value of EGl at 10 GHz is $\varepsilon' = 3.38$ and $\tan\delta = 0.15$, which when injected into grooves of silicone substrate will increase the ε_{eff} and is desirable for the compensating the right shift.

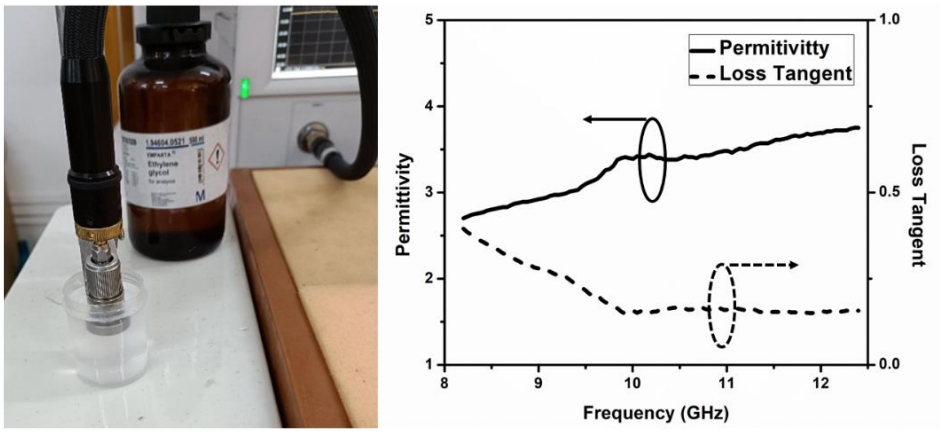

Figure 3.2 (a) Permittivity studies in X-band using dielectric probe kit and (b) measured permittivity and loss tangent of Ethylene Glycol (EGl) in X-band

3.2.2 Substantiation of variation in dielectric constant of the injected substrate

Microwave dielectric characterization of groove incorporated silicone rubber composites are carried out at X-band frequency region with transmission–reflection method using Nicholson-Ross-Weir (NWR) technique as detailed in Section 2.5 of Chapter II [5, 6]. A 3D printed mould with the dimension similar to X-band waveguide i.e. (22.86 × 10.16) mm^2 is used to develop the prototype, as in Figure 3.3(a) and 3.3(b). Three prototypes viz., silicone without any groove, silicone with air filled groove and silicone with EGl filled groove, are measured using this technique. The thickness of the material prototypes is kept at 2mm, which is same as the thickness of substrate on which antenna will be developed. A groove of diameter, D_g=1mm is centred within the substrate. D_g > 1mm affects the mechanical strength of the substrate while lower values of D_g are difficult to fabricate.

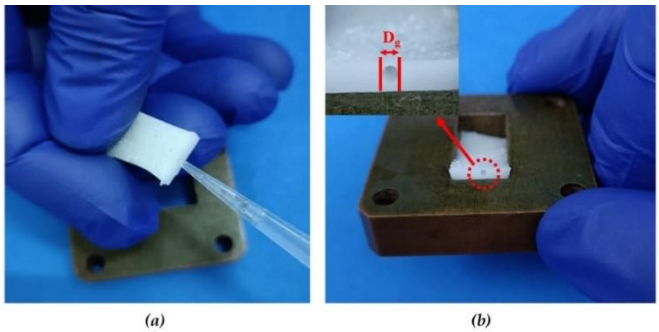

Figure 3.3 (a) Groove incorporated silicone injected with EGl and (b) silicone with empty groove i.e., air filled

The effective permittivity of the silicone rubber increases with incorporation of EGl in the groove and decreases when the groove is filled with air as compared with the silicone rubber without any groove, refer Figure 3.4(a). The loss tangent values, Figure 3.4(b), are not affected to that extent by injection of the fluids in the silicone material.

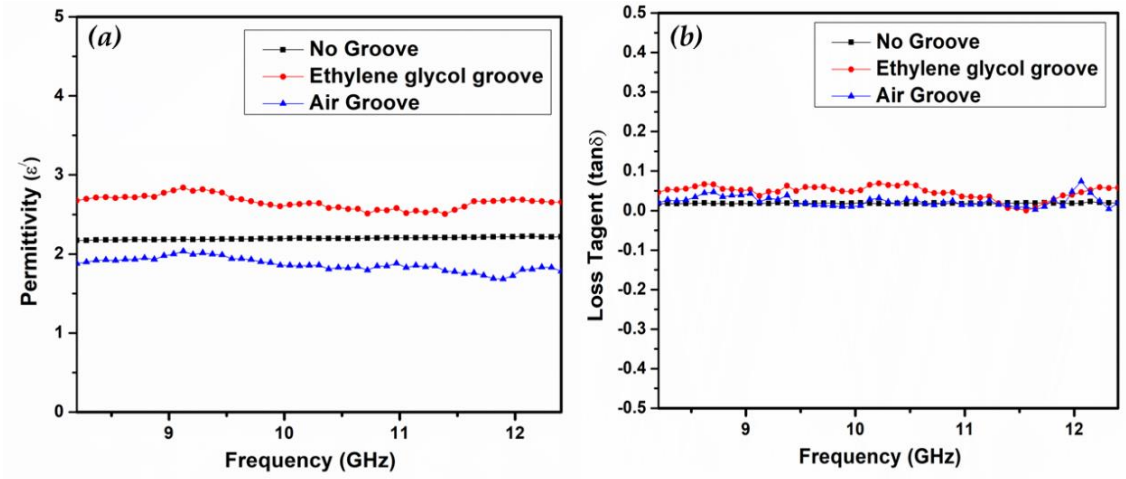

Figure 3.4 Measured (a) permittivity and (b) loss tangent of silicone rubber material prototypes

3.2.3 Shape variation of grooves with bending

A shape variation of the cross section of the grooves will take place with respect to different bending radii. The modified groove integrated substrate is intended for patch antenna applications wherein the metal layers are present on the top and bottom of the substrate. While bending, these metal layers will influence the lateral forces of the substrate and hence ultimately effect the variation in the shape of the groove. Thus, a prototype is used in the current study which includes the silicone-foam substrate with a groove centred along the substrate and copper sheet attached to the either surface, Figure 3.5(a). The dimension of the prototype is 40 x 40 x 2 mm which is identical to the dimensions of the antenna to be studied in the subsequent sections.

As the substrate is bent, the lateral force along the top and bottom surface of the substrate will enforce a change in the shape of the cross section of the groove from a circular to an approximately elliptical as shown in Figure 3.5(b). The change in

the shape while bending of the substrate in turn may induce some changes in the ε_{eff} which eventually will affect the frequency shift.

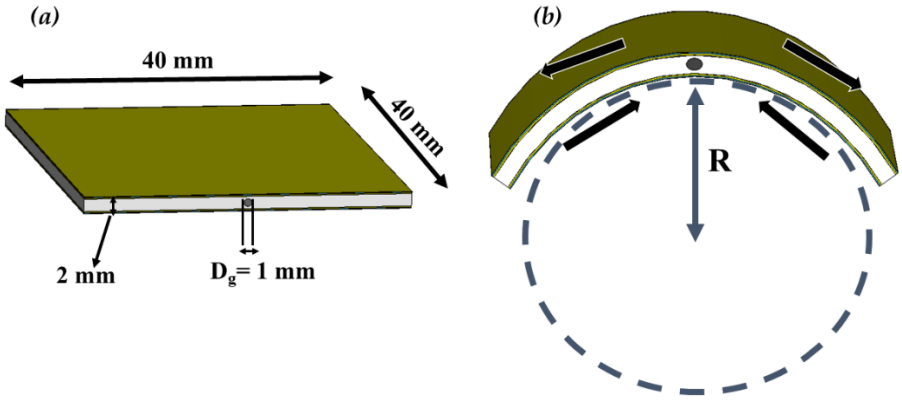

Figure 3.5 (a) Dimension of the prototype and (b) bending curvature schematic

A quantitative study to this effect is carried out by changing the bending radii and measuring the change in the shape in terms of the eccentricity of the groove, e_g, i.e., ratio of the major axis length and minor axis length of the cross section. The metallized substrate is placed over semicylindrical moulds of different radii (R= 40mm, 30mm and 20mm) and observation taken using a travelling microscope with a least count of 0.01mm. The arrangement is shown in Figure 3.6.

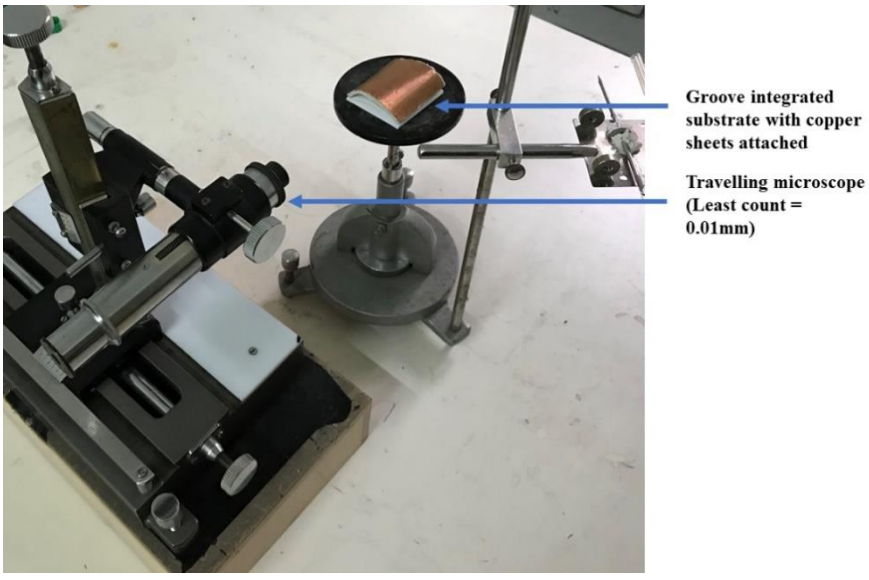

Figure 3.6 Travelling microscope arrangement for studying the variation in shape of grooves with bending

The photographic grayscale image captured through the cross-wire scope of the travelling microscope depicting the variation in e_g is shown Figure 3.7.

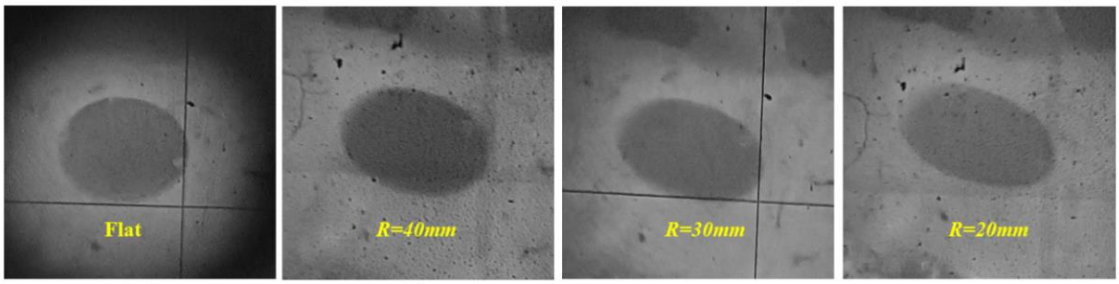

Figure 3.7 Grayscale images of the groove as observed through the travelling microscope depicting the variation in e_g with R

With bending the cross section of circular groove changes to elliptical with increase in e_g from ~1.03 to ~1.55, as tabulated in Table 3.1.

Table 3.1 Quantification of variation in shape of cross section of grooves

Bending Radius (R) - mm	*Major axis length (mm)*	*Minor axis length (mm)*	*Eccentricity of the groove (e_g)*
Flat	*1.03*	*1.00*	*1.03*
40	*1.19*	*0.98*	*1.21*
30	*1.32*	*0.96*	*1.37*
20	*1.45*	*0.93*	*1.55*

3.3 SIMULATION STUDY

Simulations are carried out with CST Microwave Studio on antenna designed on grooved silicone foam substrate by importing dielectric parameters at 10 GHz from Figure 3.4 and e_g from Table 3.1. Two approaches – XZ bending (Topology I) and YZ bending (Topology II) are studied separately.

3.3.1 Topology I-Bending perpendicular to the radiating edge (XZ-Bending)

The antenna is designed in such a way that the groove is perpendicular to the radiation edge of the patch as shown in the Figure 3.8.

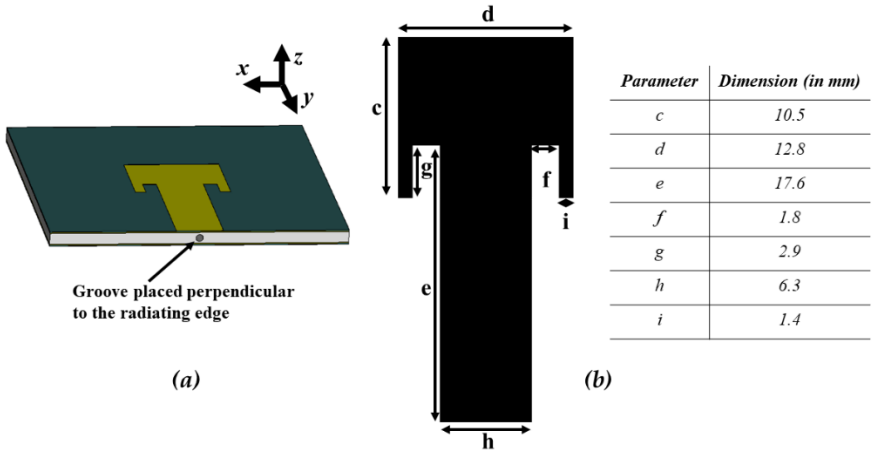

Parameter	*Dimension (in mm)*
c	*10.5*
d	*12.8*
e	*17.6*
f	*1.8*
g	*2.9*
h	*6.3*
i	*1.4*

Figure 3.8 (a) Antenna Topology-I and (b) schematic of patch with microstrip feed line along with dimensions

The bending of the antenna in this case shifts the frequency towards the lower side and hence the groove in this antenna is filled with air to decrease the $\varepsilon_{eff.}$ For every bending angle the minor axis and major axis length is fed into the simulator model from Table 3.2. The obtained S_{11} plot is as shown in Figure 3.9.

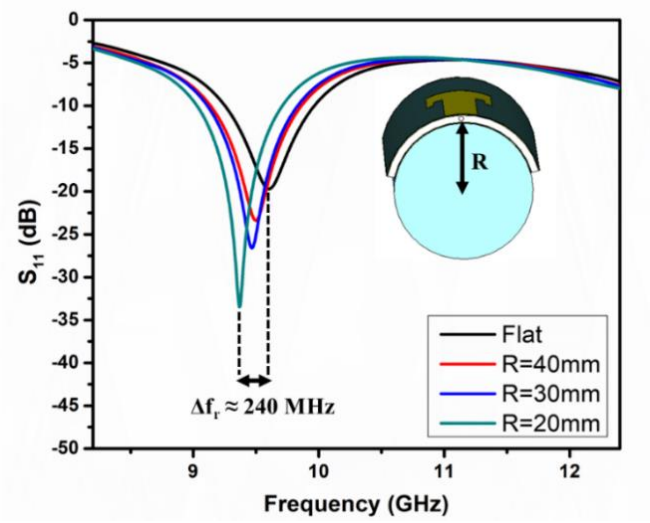

Figure 3.9 Simulated S_{11} plot with variation in bending radii (flat, 40mm, 30mm and 20mm) of Topology I antenna system and simulated structure (inset).

The S_{11} characteristics plotted in Figure 3.9 exhibits a maximum value of frequency shift, Δf_r , of 240 MHz when the antenna is bent up to a bending radius of 20mm. In the previous study, refer Chapter II Section 2.5, a shift of 220 MHz was observed

when the antenna was bent up to 20mm without the presence of grooves. Thus, no significant compensation could be observed by inclusion of a single groove.

3.3.2 Topology II – Bending parallel to the radiating edge (YZ-Bending)

The antenna patch in this topology is placed in a way such that the width of the patch is parallel to the length of the grooves as shown in the Figure 3.10. The patch dimensions are optimized to resonate at around 10 GHz.

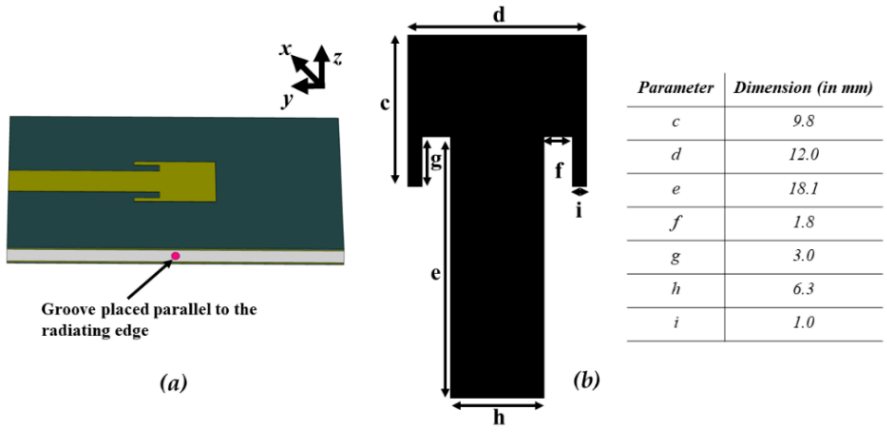

Parameter	*Dimension (in mm)*
c	*9.8*
d	*12.0*
e	*18.1*
f	*1.8*
g	*3.0*
h	*6.3*
i	*1.0*

Figure 3.10 (a) Antenna Topology-II schematic and (b) parameters and dimensions of patch with feed line

As seen from Figure 3.11, $\Delta f_r \approx 310$ MHz, whereas for the similar configuration of bending without any grooves (Chapter II, Section 2.5) the maximum value of frequency shift was 90 MHz, which is contrary to what was intended.

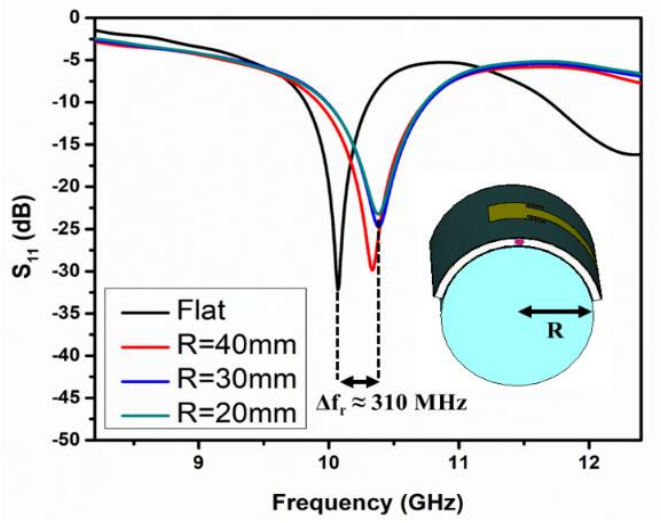

Figure 3.11 Simulated S_{11} plot with variation in bending radii (flat, 40mm, 30mm and 20mm) of Topology II antenna and simulated structure (inset)

3.3.3 Optimization of the groove count

In the preceding section, it has been observed that a single groove does not have desirable compensation effect. Further optimization is carried out by increasing the groove counts. The increase is done in even multiples to either side of the central groove in order to maintain the symmetry of the structure. The distance between the grooves, *B*, is also varied to study their effect in the S_{11} characteristics. The initial value of *B* is taken to be 2 mm due to fabrication constraints and increased in steps of 1 mm to a maximum value which is governed by the empirical relation

$$B(max) \approx \frac{d-D_g}{n-1} \qquad (3.1)$$

where, *n* is the groove count and *d* is the width in case of Topology I and length of the patch in case of Topology II and D_g is the diameter of the grooves. This constraint in *B* has been derived from the results of the optimization, wherein, it is found that the effect of the grooves ceases when we consider distance between the grooves at the extreme end to be greater the patch dimensions. The simulation is carried out for both topologies.

Topology I

3 groove counts

As seen from Figure 3.12(a-d), as *B* is incremented the Δf_r follows a decreasing trend, being lowest (110MHz) for $B = 5mm$ for which the grooves are underlying from edge to edge of the patch. Beyond which, Δf_r increases as obvious from Figure 3.12(e).

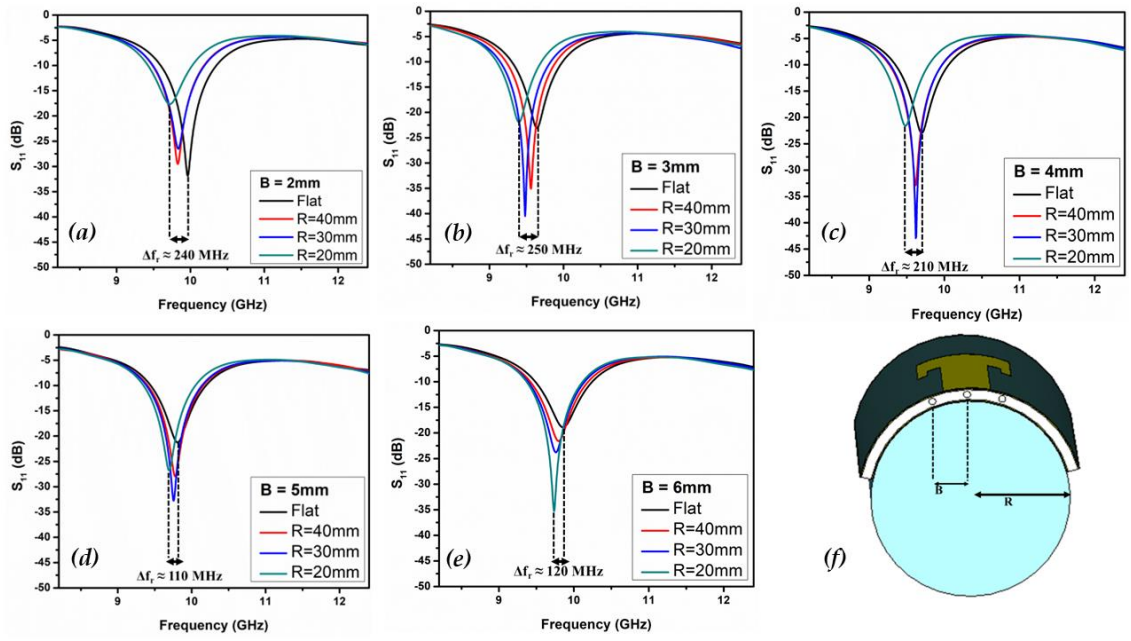

Figure 3.12 Simulated S_{11} plot of Topology I antenna with three grooves studied at bending radii (flat, 40mm, 30mm and 20mm) and varying groove distance, *B*= (a) 2mm, (b) 3mm, (c) 4mm, (d) 5mm, (e) 6mm and (f) simulated structure

5 groove counts

In the next step, the number of grooves is increased to 5 and the distance between the grooves, *B*, are studied for two instances viz., 2mm and 3mm following the Equation (3.1). The results are plotted in Figure 3.13. As can be seen that, herein also Δf_r decreases to 80 MHz for $B= 3mm$, i.e., when the hindmost grooves are lying at the extreme patch edges.

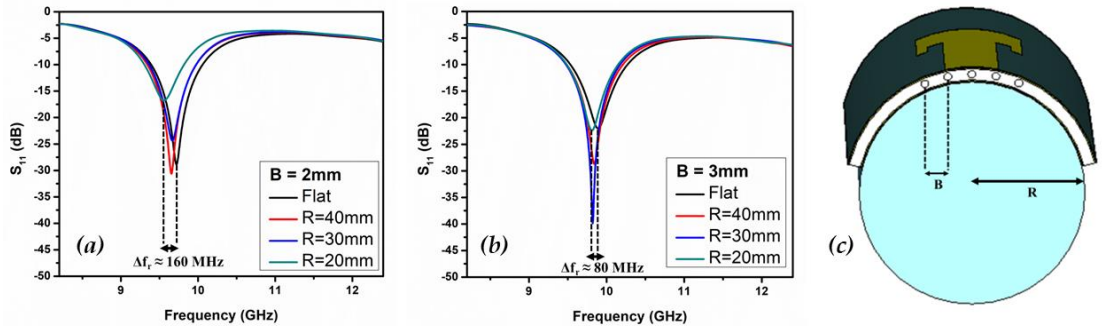

Figure 3.13 Simulated S_{11} plot of Topology I antenna with five grooves studied at bending radii (flat, 40mm, 30mm and 20mm) and varying groove distance, *B*= (a) 2mm, (b) 3mm and (c) simulated structure

7 groove counts

S_{11} plot in Figure 3.14 is for the antenna with 7 grooves, with B = 2mm only. As can be seen Δfr reduces to 40 MHz. The study was carried out for all the bending radii of 40mm,30mm and 20mm. It is observed that frequency shift for 20- and 30-mm bending radii is 30 MHz, whereas for 40mm bending it is 40 MHz.

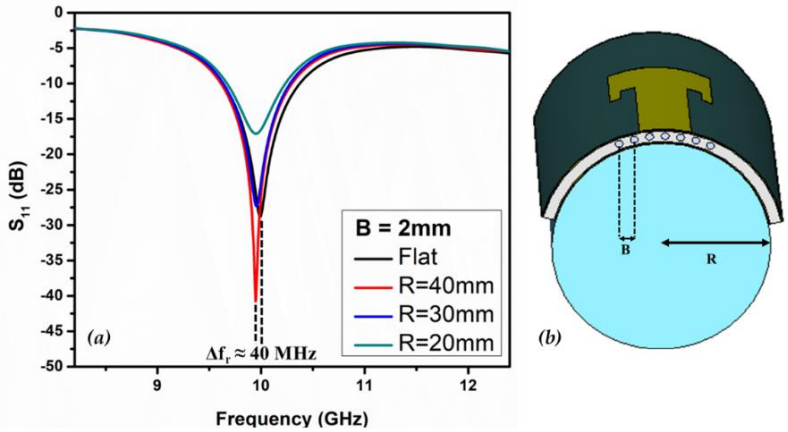

Figure 3.14 (a) Simulated S_{11} plot of Topology I antenna with seven grooves studied by variation in bending radii (flat, 40mm, 30mm and 20mm) and with groove distance B = 2mm (b) simulated structure

Further, on increasing the number of grooves to nine, the hindmost grooves cross over the patch edge, showing no significant change in Δf_r and hence has not been considered in the study.

The antenna with the seven grooved configuration in flat profile has -10 dB bandwidth of the ~ 7.4% i.e., ±36 MHz of the resonant frequency, which is approximately equal to the shift observed for all the bending radii. Thus, this structure with 7 grooves and with a B = 2mm can be considered as the optimized configuration for Topology I and will be fabricated, tested for obtaining its measured antenna parameters.

Field analysis

The electric field distribution with seven grooved configuration is plotted at the resonant frequency. The flat and bent profile is plotted in the contour form as shown in Figure 3.15(a-d). The plane for the contour plot is taken to be the cross-sectional plane parallel to the radiating edge of the antenna so as to observe the

field distribution along the cross section of the grooves. It can be seen that the electric field protrudes away from the patch as the antenna is bent. Additionally, it is observed that, the intensity of the electric field reduces as we move away from the grooves at both the extreme ends. The results agree with the findings of the optimization study, wherein increasing the number of grooves or increasing B beyond its maximum value following Equation (3.1) does not have any constructive effect in reducing the frequency shift.

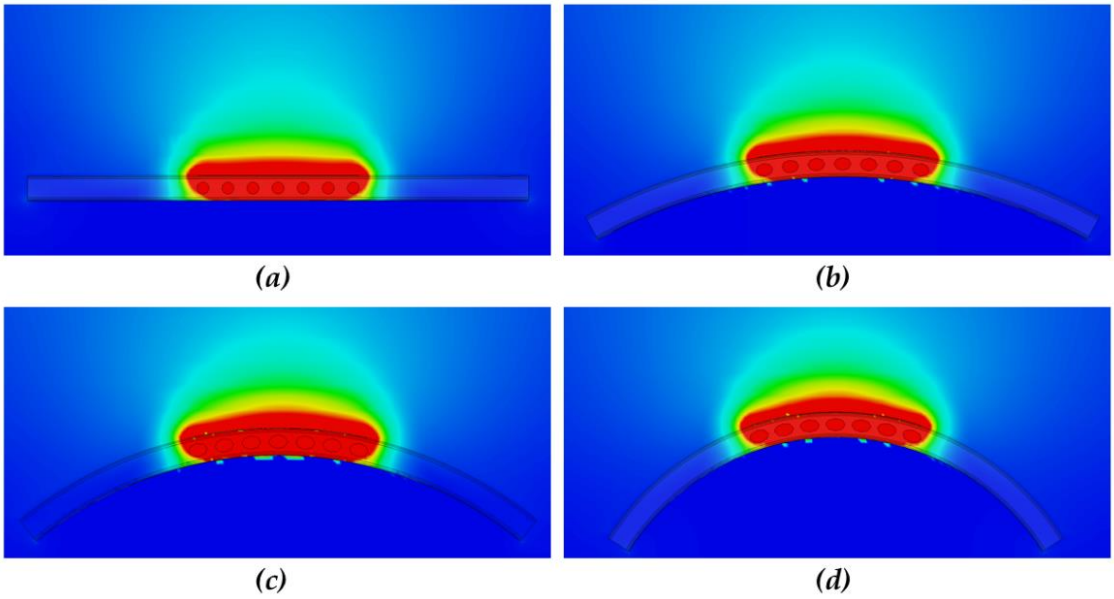

Figure 3.15 Electric field distribution (contour) along the plane parallel to the radiating edge of the Topology I antenna for (a) flat and R = (b) 40 mm, (c) 30 mm and (d) 20 mm

Topology II

3 groove counts

With 3 grooves, as B is varied, Δf_r, decreases from 230 MHz (B = 2mm) to 160 MHz (B = 4mm) Figure 3.16(a-c) and thereafter increases for B = 5mm. This limiting value of B is also accorded in Equation (3.1).

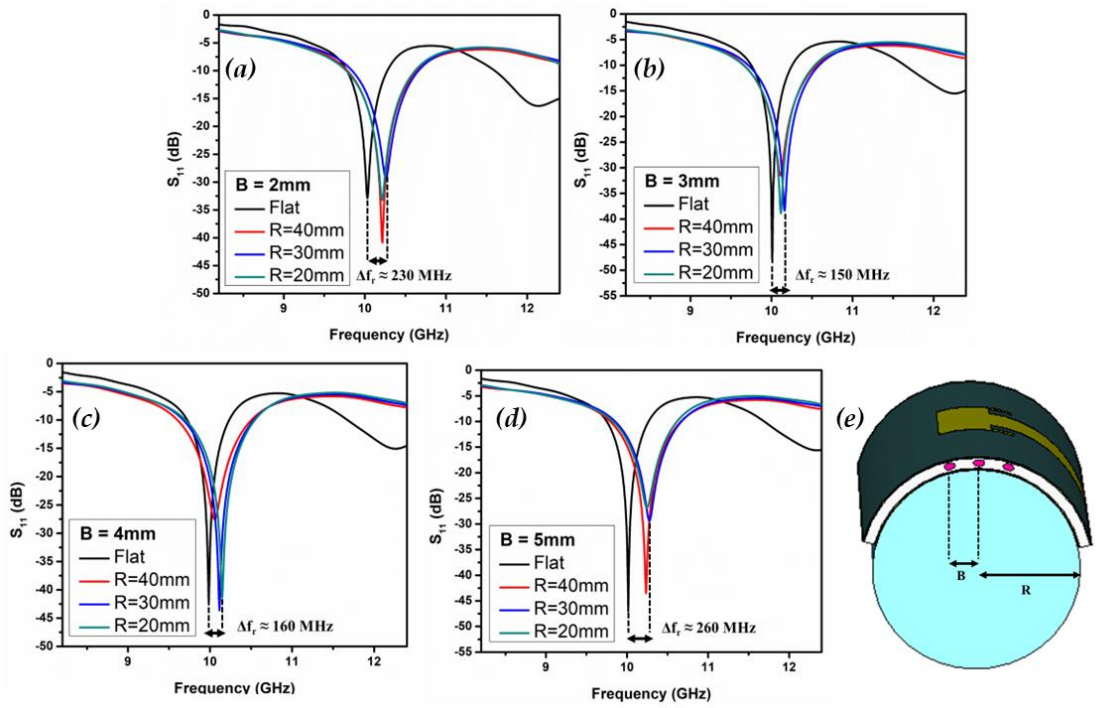

Figure 3.16 Simulated S_{11} plot of Topology II antenna with three grooves studied by variation in bending radii (flat, 40mm, 30mm and 20mm) and groove distance *B*= (a) 2mm, (b) 3mm, (c) 4mm, (d) 5mm and (e) simulated structure

5 groove counts

For 5 grooves, the Δf_r is 70 MHz for B = 2mm, Figure 3.17(a), and then increases to 160 MHz for B = 3 mm, refer Figure 3.17(b).

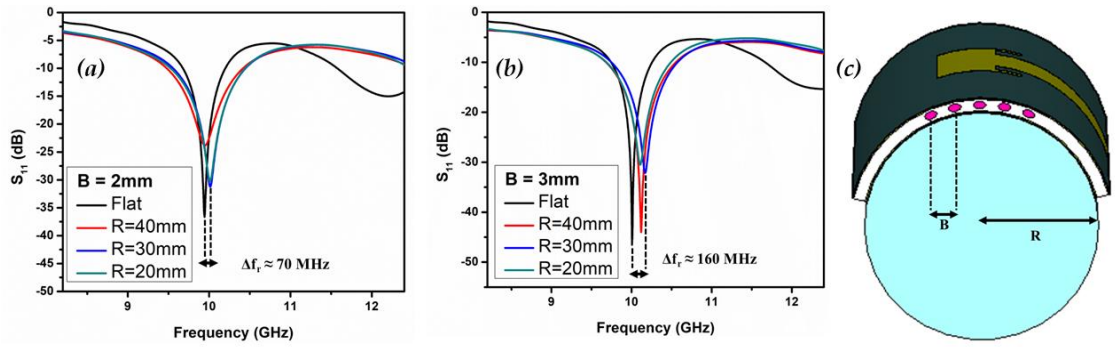

Figure 3.17 Simulated S_{11} plot of Topology II antenna with five grooves studied by variation in bending radii (flat, 40mm, 30mm and 20mm) and groove distance B = (a) 2mm, (b) 3mm and (c) simulated structure

7 groove counts

For seven grooves, refer Figure 3.18, simulation is carried out for B = 2mm, which is in accordance with Equation (3.1). The Δf_r in found to be 40 MHz.

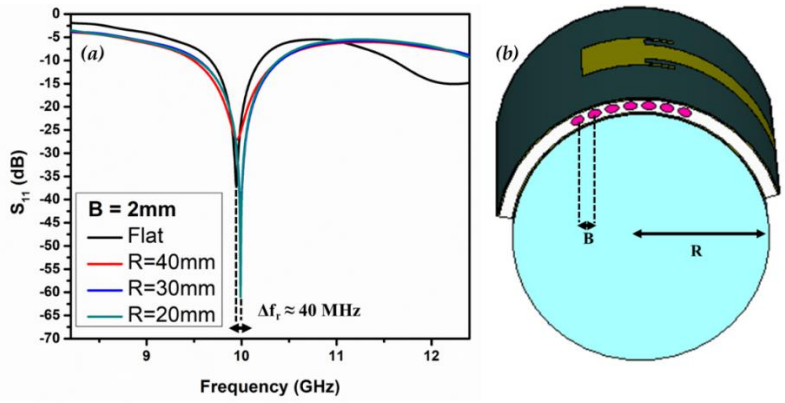

Figure 3.18 (a) Simulated S_{11} plot of Topology II antenna with seven grooves studied by variation in bending radii (flat, 40mm, 30mm and 20mm) and groove distance B = 2mm and (b) simulated structure

Thus, with increase in the groove count from one to seven, the maximum value of shift in the frequency i.e., Δf_r, reduces from 310 MHz to 40 MHz. The -10 dB bandwidth of the antenna with 7 grooves in flat condition shows that the bandwidth is the ±25 MHz about the centre frequency while the maximum shift is +40MHz.

Therefore, for Topology II, with seven groove configuration with B = 2mm may be considered as the optimized structure. In the succeeding section, the patch antenna with seven grooves embedded are fabricated for both the topologies and its performance studied.

Field Analysis

The electric field distribution at the resonant frequency for seven grooves configuration for flat and bent profile is plotted in the contour form as shown in Figure 3.19(a-d). Herein, the plane for the contour plot is taken to be the cross-sectional plane parallel to the non-radiating edge of the antenna. Unlike Topology I, the electric field distribution gets restricted within the patch as the antenna is

bent. Also, it can be seen clearly that beyond the grooves at the extreme ends the field intensity reduces.

A small hump corresponding to the feedline radiation is observed in the electric field distribution, Figure 3.19.

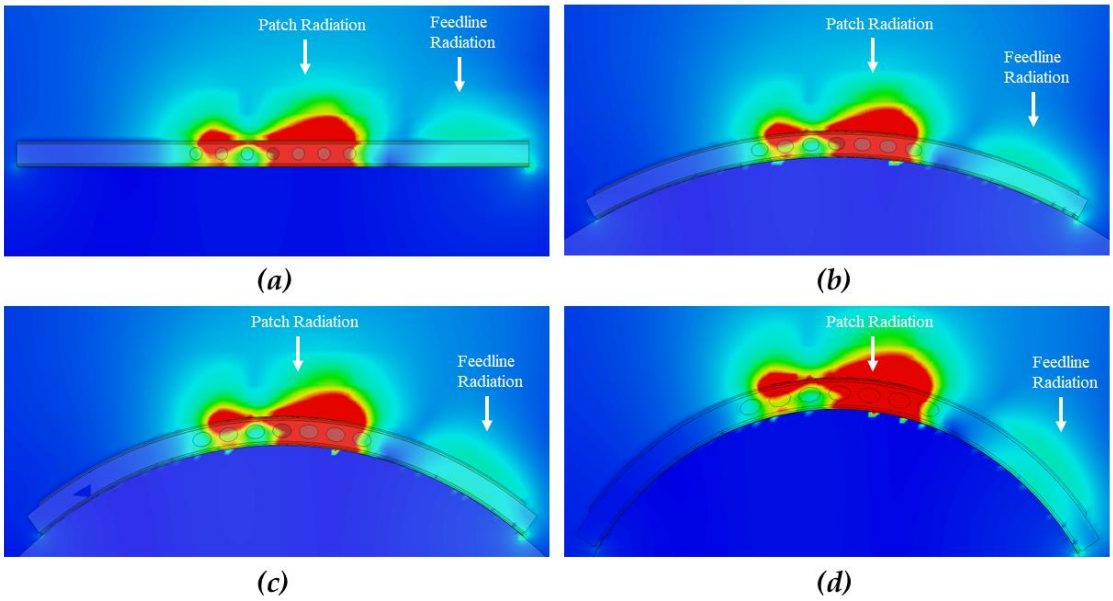

Figure 3.19 Electric field distribution (contour) along the plane parallel to the non-radiating edge of the Topology II antenna for (a) flat and R = (b) 40 mm, (c) 30 mm and (d) 20 mm

3.4 EXPERIMENTAL STUDY

In simulation, the seven grooved substrate yielded the optimized result for both the bending directions in terms of minimizing the frequency shift. The experimental validation is carried out by realizing the antenna on seven grooved substrate and testing its performance with varying bending radii.

3.4.1 Realization of the groove substrate

A special PLA mould is 3D printed (BoxzY, USA) as shown in the Figure 3.20(a) for the 7 grooved substrate structure. The mould is dimensioned to fabricate semi cylindrical grooved one-half of the substrate structure. The outer surface of one-half substrate is then attached to a Poly-Urethane (PU) foam layer using the technique described in Section 2.3 of Chapter II as shown in Figure 3.20(b).

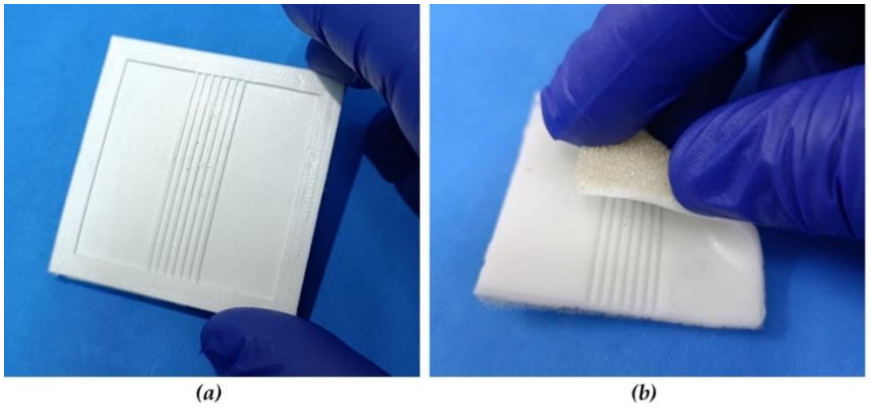

Figure 3.20 (a) 3D printed PLA mould to fabricate one half of the substrate and (b) substrate moulded with semi cylindrical grooves and attached with PU-foam

Two such halves, thereafter, are prudently aligned and cemented together using silicone rubber-based adhesive to obtain the cylindrical groove incorporated substrate of dimension 40mm x 40mm x 2mm (Figure 3.21).

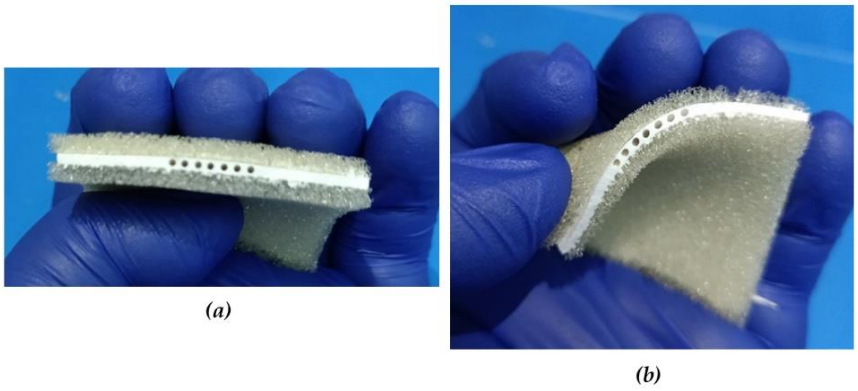

Figure 3.21 Fabricated silicone-foam substrates with grooves

The artwork is etched as per the dimensions given in Figure 3.8(b) and 3.10(b), on a copper sheet of thickness 0.03 mm and is attached on the outer surface the groove incorporated substrate. Care is taken such that the centre axis of the patch is aligned with the centre of the substrate. A sheet of same thickness is attached as the ground plane to the other side of the substrate. For Topology I, the orientation of the patch is such that the grooves are along the non-radiating edge, while for Topology II the grooves lie parallel to the radiating edge. The seven cylindrical grooves are kept hollow i.e., air-filled in case of Topology I antenna, Figure 3.22(a), and for Topology II EGl is injected using a micro pipette, Figure 3.22(b). The liquid

filled grooves enacts like capillaries and the surface tension of the liquid confines it within the grooves thus exterminating the need of sealing the grooves.

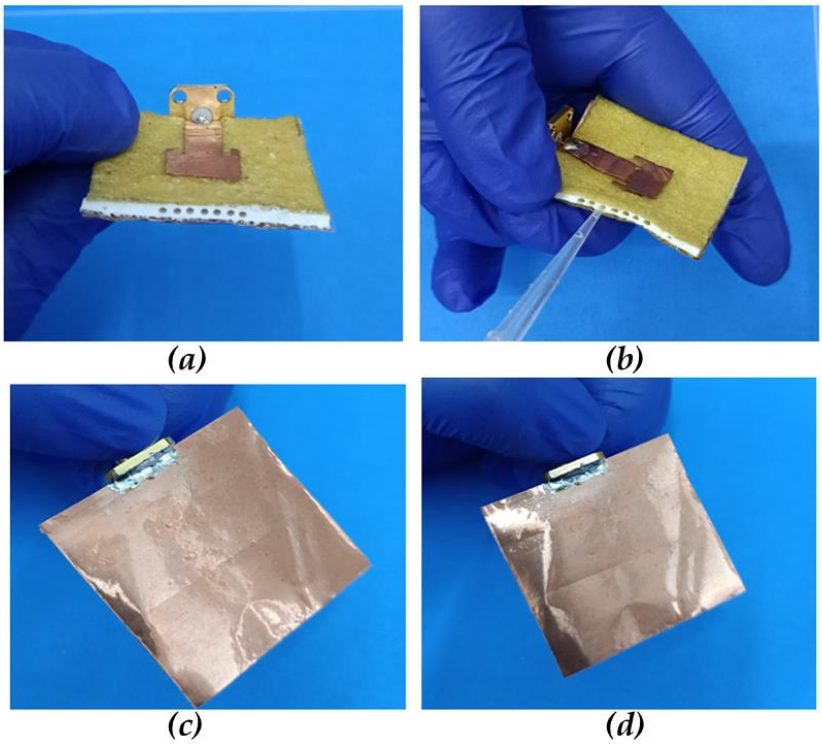

Figure 3.22 Fabricated patch antenna (a) Topology I with air filled grooves, (b) Topology II with EGl filled grooves, (c) rear view of the Topology I patch antenna and (d) rear view of the Topology II patch antenna

3.4.2 Antenna performance studies

The antennas are characterized for its resonating ability (S_{11}) and radiation capability using the test set up as mentioned in Section 2.6.1 in Chapter II. The radiation measurements are carried out along two orthogonal broadside planes. Study of the effect of bending on the antenna characteristics is carried by placing the antenna on 3D printed PLA material semi cylinders of radii 40 mm, 30mm and 20 mm, Figure 3.23(a-b).

(a) *(b)*

Figure 3.23 (a) Topology II antenna characteristics measured using radiation pattern measurement system and (b) Topology I antenna (left) bent on a 30mm PLA semi cylinder and Topology II antenna (right) bent on a 20mm PLA semi cylinder

Performance study for Topology I

Figure 3.24(a) are the S_{11} curves for the Topology I antenna bent along the XZ plane for three different bending radii viz., 40mm, 30mm and 20mm. The S_{11} curve for the flat profile of the antenna is plotted for reference. Figure 3.24(b) are the same set of curves with the frequency range being expanded. It is seen that the frequency shift for 40mm bending is ≈ 10 MHz, for 30 mm it is ≈ 20 MHz and for 20 mm it is ≈ 30 MHz towards the lower side with respect to the flat profile. The -10 dB percentage bandwidth increases with bending. Moreover, the S_{11} values (in dB) becomes more negative indicating better impedance matching with bending.

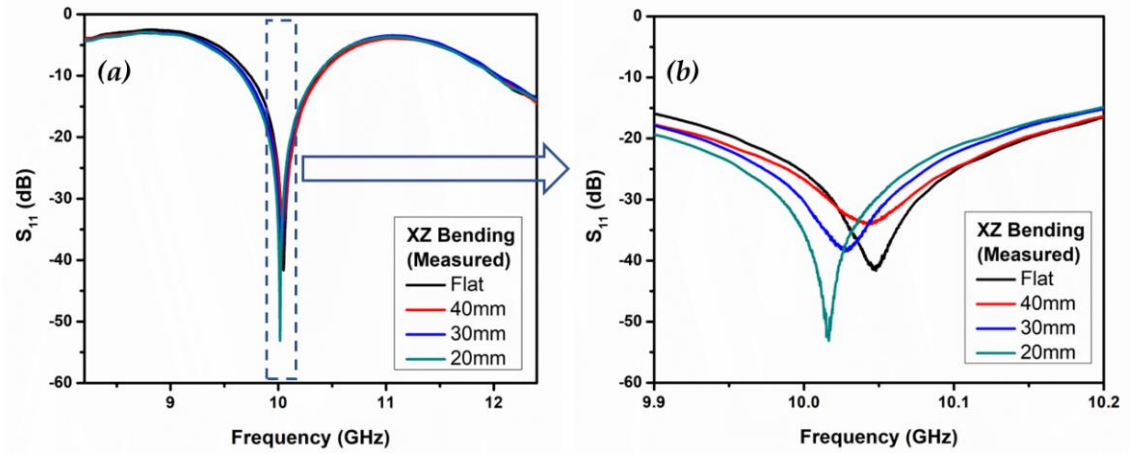

Figure 3.24 (a) Measured S_{11} plots for different bending radii of the Topology I antenna in X-band and (b) frequency range expanded (9.9-10.2 GHz)

Figure 3.25(a) defines the bending plane and the red circle indicates the XZ radiation pattern plane.

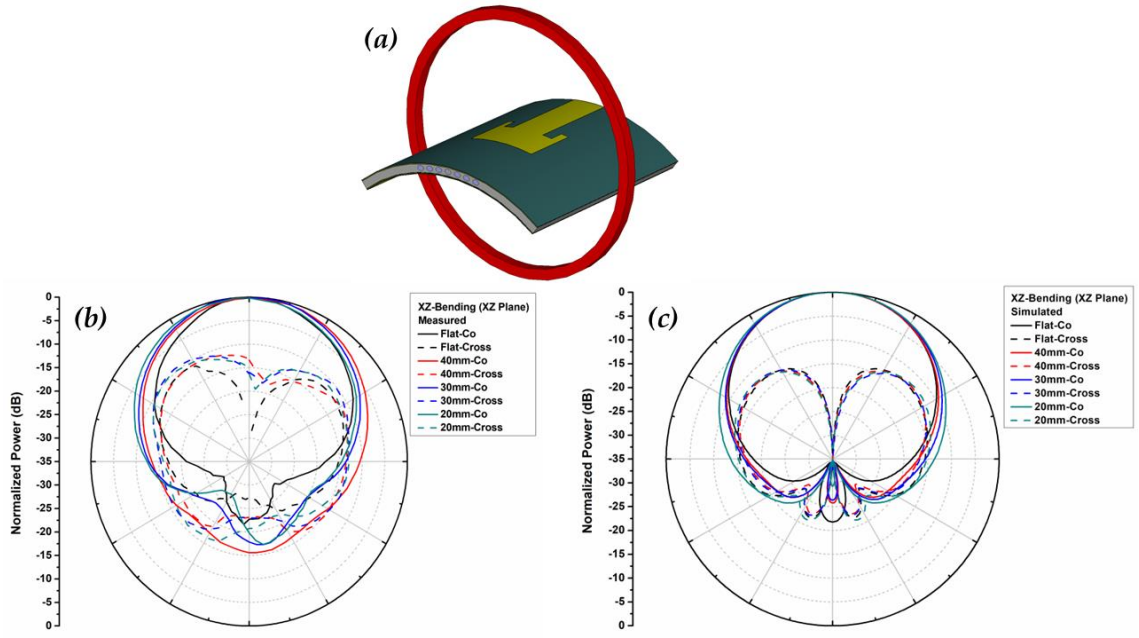

Figure 3.25 (a) Schematic of the Topology I antenna bent along the XZ plane with the red circle indicating the XZ radiation plane, (b) measured normalized radiation pattern and (c) simulated normalized radiation pattern

The measured normalized radiation pattern plots, Figure 3.25(b), show that with bending the co polar patterns gets broadened. The cross polar patterns have magnitude lower than the corresponding co polar ones, and the bending also has an effect in increasing the magnitude of the cross polar levels. Similar trend is observed in the simulated patterns, Figure 3.25(c).

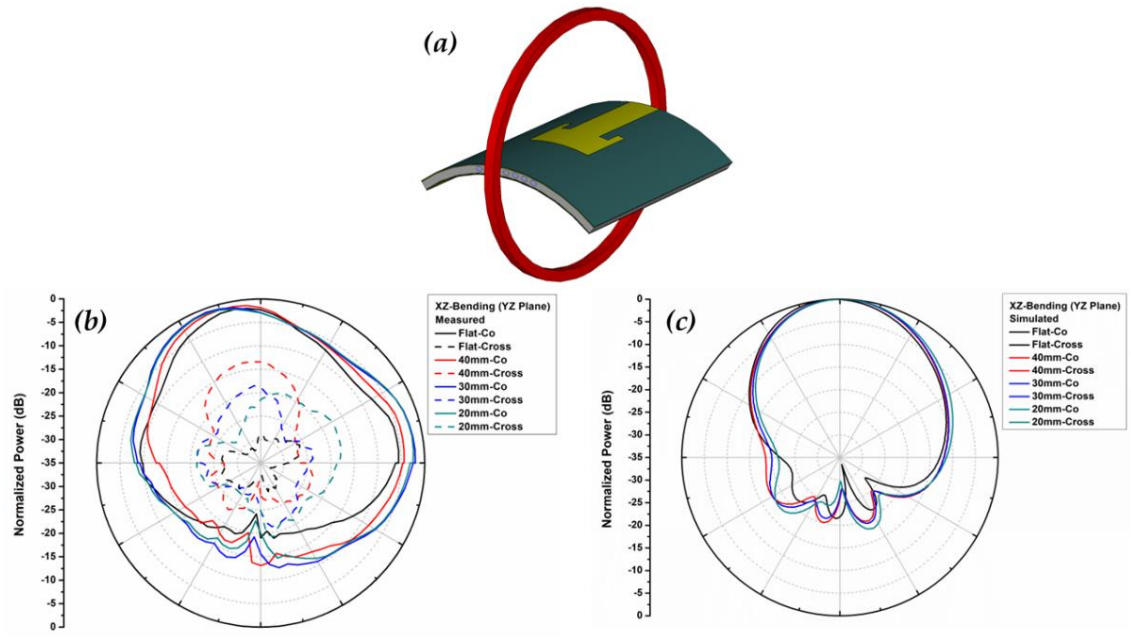

Figure 3.26 (a) Schematic of the Topology I antenna bent along the XZ plane with the red circle indicating the YZ radiation plane, (b) measured normalized radiation pattern and (c) simulated normalized radiation pattern

The YZ plane radiation patterns include radiations from the feedline which leads to broader patterns on the end-fire direction as depicted in the pattern. In the broadside direction, Figure 3.26(b), not much change in the patterns is observed. The back lobe levels however, in both XZ and YZ plane enhances. Also, the cross polar level of the antenna in YZ plane are much below the corresponding co-polar levels and hence the plots are not visible within the range as evident from Figure 3.26(c).

Performance study for Topology II

The S_{11} plots for Topology II have been shown in Figure 3.27(a) and the expanded plot of the same in Figure 3.27(b). The frequency shift for 40mm bending along the YZ plane is ≈ 40 MHz, for 30 mm bending it is ≈ 80 MHz and for 20 mm bending it is ≈ 110 MHz towards the higher side with respect to the flat profile. The -10 dB percentage bandwidth decreases by approximately 3% with bending upto 20 mm radii.

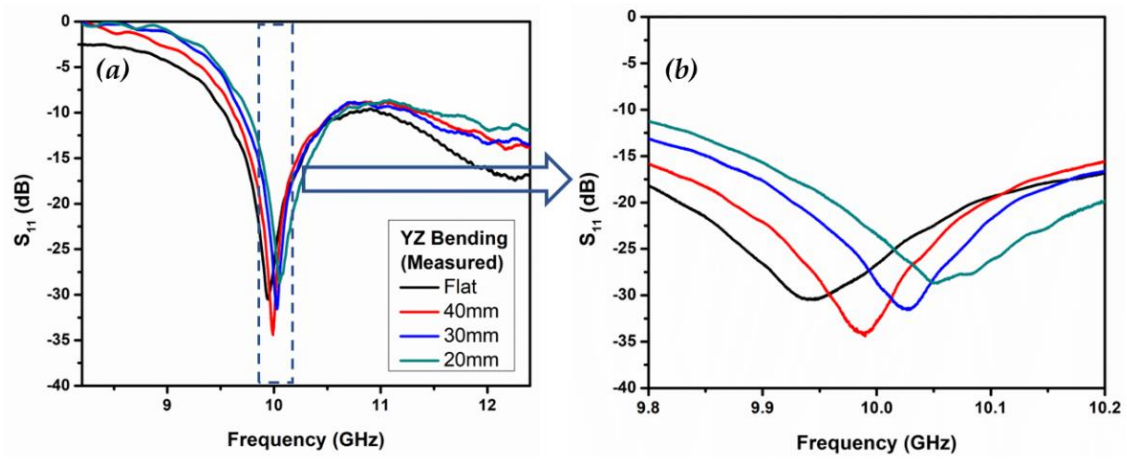

Figure 3.27 (a) Measured S_{11} plots for different bending radii of the Topology II antenna in X-band and (b) frequency range expanded (9.8-10.2 GHz)

The normalized radiation pattern plots for YZ bending and XZ radiation plane are shown in Figure 3.28 and YZ radiation plane are shown in Figure 3.29. The co-polar patterns for both the radiation planes exhibit a broadening effect as compared to the flat case along with increase in back lobe levels. The magnitude of the cross polar levels also increases with bending.

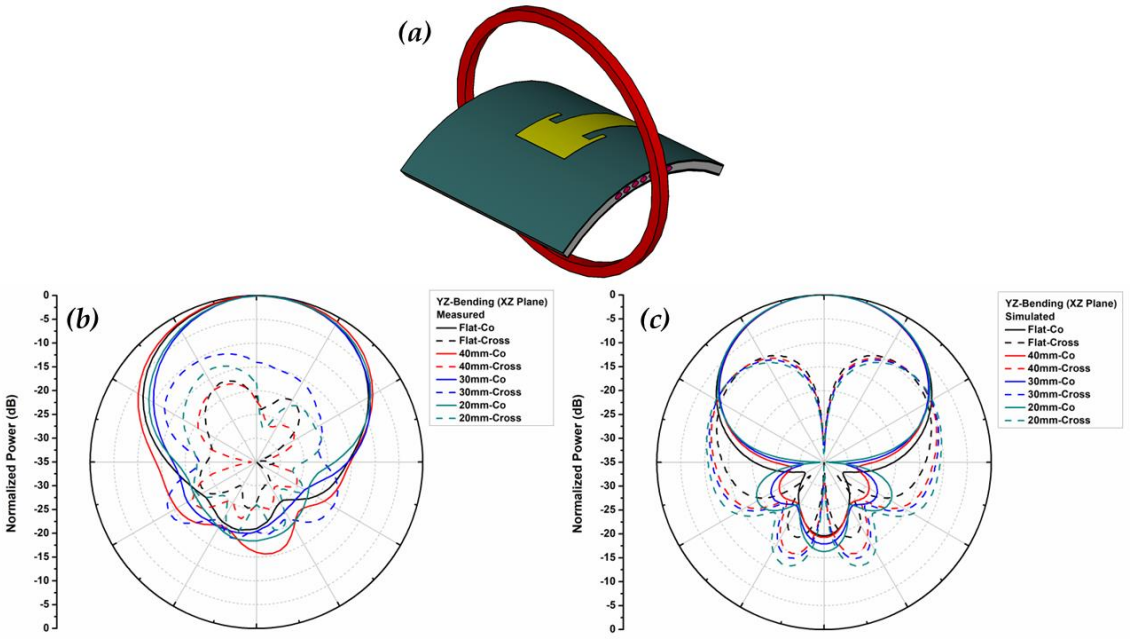

Figure 3.28 (a) Schematic of the Topology II antenna bent along the YZ plane with the red circle indicating the XZ radiation plane, (b) measured normalized radiation pattern and (c) simulated normalized radiation pattern

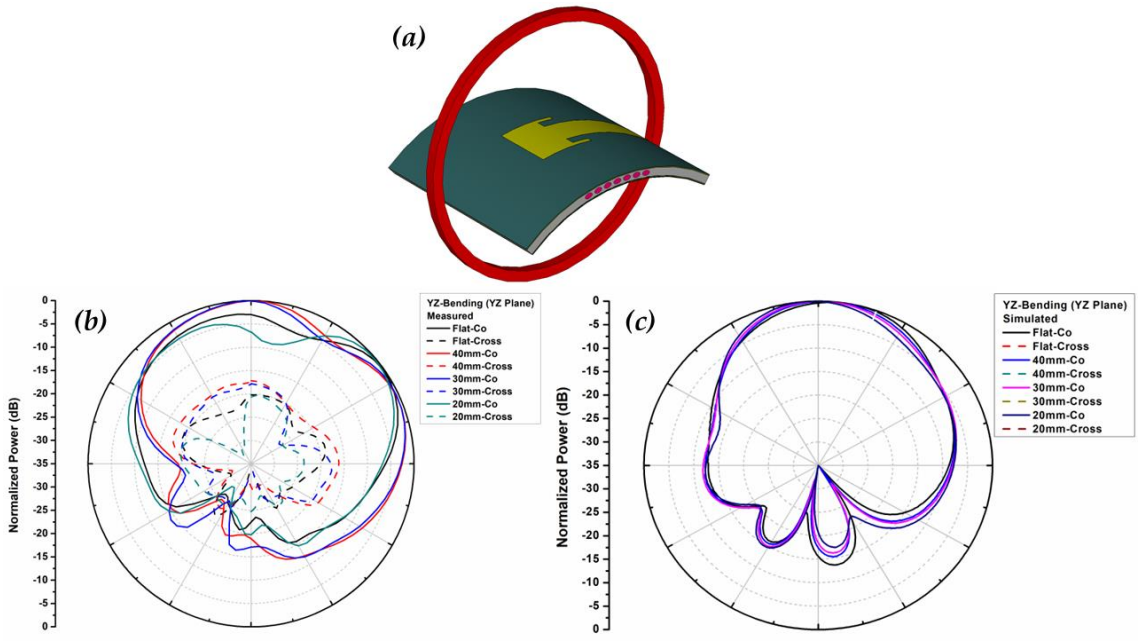

Figure 3.29 (a) Schematic of the Topology II antenna bent along the YZ plane with the red circle indicating the YZ radiation plane, (b) measured normalized radiation pattern and (c) simulated normalized radiation pattern

3.5 DISCUSSIONS

3.5.1 Analysis of antenna performance with bending

The effect of bending is examined by summarizing the results in Table 3.2. Gain, directivity and -10dB bandwidth are included. The results from the simulation study for the seven grooved structure is also included.

Some interesting trends are observed from the data. When bending takes place, the current distribution shifts towards the edges and less current accumulates at the centre of the patch [7, 8, 9] leading to a broadening of the pattern. A similar broadening of the radiation pattern is observed in Figure 3.25, 3.26, 3.28 and 3.29. Thus, as per the Equation (3.2) [10], the directivity decreases alongside the gain.

$$Directivity\ (dB) = \frac{41253}{\Theta\ X\ \Phi} \qquad (3.2)$$

where Θ and Φ are the -3dB beamwidth of the broadside orthogonal radiation patterns.

The decrease in the values of directivity and gain for both the topologies with decrease in the bending radii are obvious from the Table 3.2.

Table 3.2 Quantitative summary of the antenna characteristics in flat profile (unbent) and bent profiles

Profile	*Bending Radii (mm)*	*Resonant Frequency (GHz)*	*S_{11} (dB)*	*-10 dB % BW*	*Directivity (dBi)*	*Gain (dBi)*	*Resonant Frequency (GHz)*	*S_{11} (dB)*	*-10 dB % BW*	*Directivity (dBi)*	*Gain (dBi)*
		Measured					***Simulated***				
XZ bending (Topology I)	***Flat***	*10.04*	*-41*	*6.1*	*13.9*	*8.5*	*9.99*	*-28*	*7.4*	*9.5*	*7.8*
	40	*10.03*	*-33*	*6.9*	*11.1*	*8.1*	*9.94*	*-40*	*6.8*	*9.2*	*7.6*
	30	*10.02*	*-38*	*6.5*	*11.3*	*7.9*	*9.95*	*-27*	*6.4*	*9.1*	*7.6*
	20	*10.01*	*-53*	*6.8*	*11.3*	*7.8*	*9.95*	*-17*	*5.6*	*8.7*	*7.2*
YZ bending (Topology II)	***Flat***	*9.94*	*-30*	*11.7*	*13.1*	*7.3*	*9.94*	*-37*	*5.2*	*8.2*	*6.4*
	40	*9.98*	*-34*	*9.6*	*8.1*	*7.0*	*9.95*	*-27*	*9.1*	*8.1*	*6.1*
	30	*10.02*	*-31*	*8.7*	*9.9*	*6.8*	*9.98*	*-46*	*8.4*	*8.0*	*6.1*
	20	*10.05*	*-28*	*8.6*	*10.2*	*6.7*	*9.98*	*-60*	*8.5*	*8.0*	*6.0*

Stress experienced by the patch and at the feed point are different for XZ and YZ topologies which is evident from the variation in the S_{11} and -10dB bandwidth values. The current distribution in case of XZ Topology protrudes while for YZ bending caves in (refer Figure 3.15 and 3.19), leading to variation in impedance and hence the S_{11} and corresponding -10dB bandwidth values.

There is an unavoidable difference in exciting ports in simulations from the experimental measurement leading to dissimilarities in the values. Fabrication limitation may contribute to the disparities too.

3.5.2 Investigation of performance of the self-compensating technique

Self-compensating techniques studied in this work is related with similar work on bending carried out for 'ungrooved' antenna system in Chapter II. Reduction in frequency shift for both the topologies are included in Table 3.3.

Table 3.3 Quantitative summary of the frequency shift (compensation)

Bending Radii (mm)	*Frequency Shift w.r.t antenna under flat condition in MHz*			
	XZ bending (Topology I)		***YZ bending (Topology II)***	
	With Groove	*Without Groove*	*With Groove*	*Without Groove*
40	*10*	*60*	*40*	*120*
30	*20*	*50*	*80*	*120*
20	*30*	*50*	*110*	*170*

For Topology I, at 40mm bending the frequency shift reduces 6 times as compared to the 'ungrooved' antenna with same bending radius. For maximum bending, R= 20mm, the shift reduces to nearly half. For Topology II, at 40mm of bending radius, the frequency shift is 1/3 of the shift for 'ungrooved' version while for 20mm bending it is lessened by nearly two-third.

To get an insight of electric field distribution of the grooved and 'ungrooved' antenna system both the topologies are studied for R=40mm. The top view plane of the antenna is realized for studying the variation of the field distribution around the patch. The distribution is plotted at the respective resonant frequencies as shown in Figure 3.30. For Topology I, the spread of electric field around the radiating edge of the patch is reduced in case of grooved antenna indicating a reduction in the effective electrical length as compared to its 'ungrooved' counterpart. Thus, the antenna with air filled grooves impresses a higher resonating frequency as compared to antenna without any groove when they are bent by the same degree. This essentially leads to the compensating effect since the shift is towards left. The opposite effect is seen in case of Topology II field distribution, refer Figure 3.31. In this case, the field spread is enhanced as compared to the 'ungrooved' one, increasing the effective length, and impressing a lower resonating frequency. This would lead to the compensating effect which can counter the shift when the antenna is bent in the YZ plane.

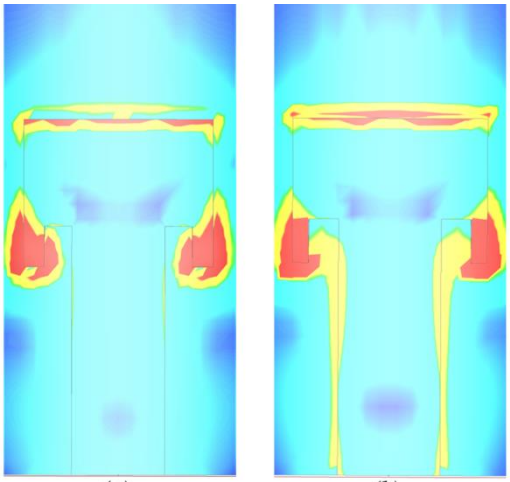

Figure 3.30 Top view of electric field distribution at the resonant frequency for 40mm bending in the XZ plane of antenna (a) with groove and (b) without groove

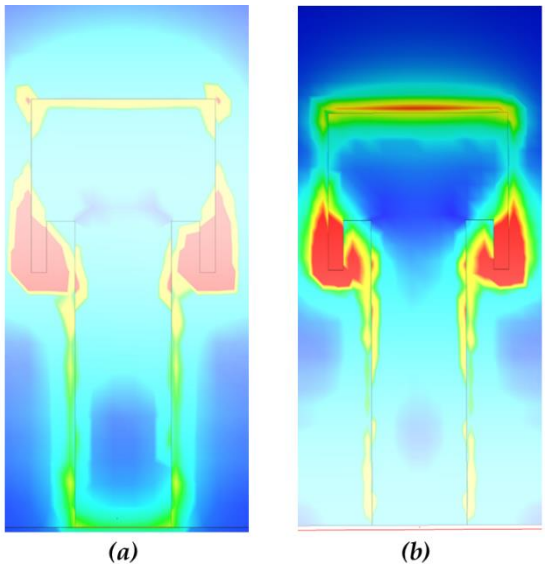

Figure 3.31 Top view electric field distribution at the resonant frequency for 40mm bending in the YZ plane of antenna (a) with groove and (b) without groove

3.6 SUMMARY

This chapter presents the design analysis and measurement of a linearly polarized microstrip patch antenna resonating in the X-band regime with a self-compensating mechanism to mitigate the detuning effects due to bending. The antenna is studied for its variation in the resonant frequency for bending radii up to 20mm and a compensation of ≈ 35-50% is achieved as compared to its

counterpart. The compensation technique is realized in real-time by altering the effective dielectric constant of the substrate by injecting dielectric fluids into the grooves incorporated in the substrate, supplemented by a shape variation of the grooves due to bending. The antennas demonstrated in the current work exhibits a gain of more than 7 dBi throughout along with a consistent -10 dB impedance bandwidth. The analysis of the electric field distribution around the patch carried out in the study ratifies the experimental findings.

References

1. Paracha, K.N., Rahim, S.K.A., Soh, P.J. and Khalily, M. Wearable antennas: A review of materials, structures, and innovative features for autonomous communication and sensing. *IEEE Access*, *7*:56694-56712, 2019.
2. Musa, U., Shah, S.M., Majid, H.A., Abidin, Z.Z., Yahya, M.S., Babani, S. and Yunusa, Z. Recent advancement of wearable reconfigurable antenna technologies: A review. *IEEE Access*, *10*:121831-121863, 2022.
3. Munawar, H.S., 2020. Reconfigurable origami antennas: A review of the existing technology and its future prospects. *International Journal of Microwave and Wireless Technologies*, *10*:34-38, 2020.
4. Long, S.A. and Huff, G.H. A substrate integrated fluidic compensation mechanism for deformable antennas. In *2009 NASA/ESA Conference on Adaptive Hardware and Systems*, pages 247-25, July 2009, IEEE.
5. Weir, W.B. Automatic measurement of complex dielectric constant and permeability at microwave frequencies. *Proceedings of the IEEE*, *62*(1):33-36, 1974.
6. Nicolson, A.M. and Ross, G.F. Measurement of the intrinsic properties of materials by time-domain techniques. *IEEE Transactions on instrumentation and measurement*, *19*(4):377-382, 1970.
7. Salonen, P., Keskilammi, M. and Rahmat-Samii, Y. Textile antennas: Effect of antenna bending on radiation pattern and efficiency. In *2008 IEEE Antennas and Propagation Society International Symposium* pages 1-4, July 2008, IEEE.
8. Zaidi, N.I., Ali, M.T., Abd Rahman, N.H., Yahya, M.F. and Nordin, M.A. Analysis on different shape of textile antenna under bending condition for GPS application. *Bulletin of Electrical Engineering and Informatics*, *9*(5), pages 1964-1970, 2020.
9. Song, L. and Rahmat-Samii, Y. A systematic investigation of rectangular patch antenna bending effects for wearable applications. *IEEE Transactions on Antennas and Propagation*, *66*(5):2219-2228, 2018.
10. Balanis, C.A. *Antenna theory: analysis and design*. John Wiley & Sons, 2016.